Icarus 277 (2016) 286–299

Contents lists available at ScienceDirect

Icarus

journal homepage: www.elsevier.com/locate/icarus

Amazonian-aged fluvial system and associated ice-related features in Terra Cimmeria, Mars

Solmaz Adeli[a,*], Ernst Hauber[a], Maarten Kleinhans[b], Laetitia Le Deit[c], Thomas Platz[d,e], Peter Fawdon[f], Ralf Jaumann[a,g]

[a] Institut fuer Planetenforschung, Deutsches Zentrum fuer Luft- und Raumfahrt (DLR), Rutherfordstr. 2, 12489 Berlin, Germany
[b] Faculty of Geosciences, Universiteit Utrecht, PO box 80115, 3508 Utrecht, The Netherlands
[c] Laboratoire de Planétologie et Géodynamique, LPG Nantes, CNRS UMR 6112, Université de Nantes, 44322 Nantes, France
[d] Max Planck Institut für Sonnensystemforschung, Justus-von-Liebig-Weg 3, 37077 Göttingen, Germany
[e] Planetary Science Institute, 1700 E Fort Lowell, Tucson, AZ 85719-2395, United States
[f] Department of Physical Sciences, The Open University, Milton Keynes MK7 6AA, UK
[g] Freie Universität Berlin, Institute of Geological Sciences, Malteserstr. 74-100, 12249 Berlin, Germany

ARTICLE INFO

Article history:
Received 25 February 2016
Revised 22 April 2016
Accepted 10 May 2016
Available online 18 May 2016

Keyword:
Mars
Surface
Climate
Ices

ABSTRACT

The Martian climate throughout the Amazonian is widely believed to have been cold and hyper-arid, very similar to the current conditions. However, ubiquitous evidence of aqueous and glacial activity has been recently reported, including channels that can be tens to hundreds of kilometres long, alluvial and fluvial deposits, ice-rich mantles, and glacial and periglacial landforms. Here we study a ~340 km-long fluvial system located in the Terra Cimmeria region, in the southern mid-latitudes of Mars. The fluvial system is composed of an upstream catchment system with narrow glaciofluvial valleys and remnants of ice-rich deposits. We observe depositional features including fan-shaped deposits, and erosional features such as scour marks and streamlined islands. At the downstream section of this fluvial system is an outflow channel named Kārūn Valles, which displays a unique braided alluvial fan and terminates on the floor of the Ariadnes Colles basin. Our observations point to surface runoff of ice/snow melt as the water source for this fluvial activity. According to our crater size–frequency distribution analysis the entire fluvial system formed during early to middle Amazonian, between ~$1.8^{+0.2}_{-0.2}$ Ga to 510^{+40}_{-40} Ma. Hydraulic modelling indicates that the Kārūn Valles and consequently the alluvial fan formation took place in geologically short-term event(s). We conclude that liquid water was present in Terra Cimmeria during the early to middle Amazonian, and that Mars during that time may have undergone several episodic glacial-related events.

1. Introduction

There is extensive geomorphological and mineralogical evidence for the presence of liquid water on the Martian surface during the late Noachian and early Hesperian epochs. This includes widespread fluvial features (e.g., Carr, 1995; Hynek et al., 2010), crater lakes (e.g., Fassett and Head, 2008), and abundant phyllosilicates in Noachian terrains (e.g., Bibring et al., 2006; Murchie et al., 2007). These features point to a different climate, most probably to a warmer and wetter environment, during early Mars as compared to the current environmental conditions. It is debated, however, how much warmer and wetter early Mars really was, and whether it was characterized by “warm and wet” (e.g., Craddock and Howard, 2002) or “cold and icy” (e.g., Wordsworth et al., 2015) conditions. The Amazonian climate, on the other hand, is globally considered as cold and hyperarid (e.g., Marchant and Head, 2007). The nature and the time frame of the transitional phase(s) into the relatively cold and dry Amazonian period remain uncertain. Morphological evidence of Amazonian liquid water, however, has been recently identified in high-resolution images of the Martian surface returned by the Mars Odyssey (MO), Mars Express (MEX), and Mars Reconnaissance Orbiter (MRO) missions. These observations revealed the presence of Amazonian-aged fluvial channels (Howard and Moore, 2011; Hobley et al., 2014; Salese et al., 2016), alluvial fans and fan deltas (Hauber et al., 2013), and very recent features including gullies (Malin and Edgett, 2000), and recurring slope lineae (RSL) (McEwen et al., 2011; Ojha et al., 2014). The remnants of Amazonian-aged tropical mountain glaciers (Head and Marchant, 2003), mid-latitude glacial deposits

* Corresponding author. Tel.: +49 3067055398.
E-mail address: solmaz.adeli@dlr.de (S. Adeli).

http://dx.doi.org/10.1016/j.icarus.2016.05.020
0019-1035/

(Gallagher and Balme, 2015), and latitude-dependent mantle (Mustard et al., 2001; Kreslavsky and Head, 2002; Head et al., 2003) point to potential recent ice ages (Head et al., 2003). Variation in spin-axis/orbital parameters (Laskar et al., 2004) during the late Amazonian may have caused the mobilization of ice from high-latitudes and its re-deposition at mid-latitudes. Local melting of these ice-rich deposits may have led to the incision of the Martian surface with channels and fluvial valley systems which would offer unique insights into the Amazonian climate, which would increase our understanding of the climatic evolution of Mars and the transition from early Mars to the recent Amazonian period.

Here we study the morphology, context, likely formative processes and duration of activity of an Amazonian-aged fluvial system, including the Kārūn Valles located in the downstream section of this system. The fluvial system is located in the Terra Cimmeria region and terminates on the floor of the Ariadnes Colles basin. We conduct the first geomorphological analysis of this fluvial system based on the analysis of MO, MEx and MRO images. Our analyses revealed the existence of very well-preserved erosional features such as incised channel beds and streamlined islands, as well as depositional features including alluvial fans and fan deltas. In order to infer potential sources of water, and the formative time frame and mechanism, we investigated the geomorphology and calculated the hydraulic parameters of this fluvial system. This will help to understand the climate at the time of formation and thus the subsequent climate development towards the current conditions.

2. Data and methods

For morphological investigations we used images acquired by the High Resolution Stereo Camera (HRSC) (Neukum et al., 2004; Jaumann et al., 2007) on board the Mars Express (MEX) orbiter and the Context Camera (CTX) (Malin et al., 2007) on board the Mars Reconnaissance Orbiter (MRO), which have typical ground resolutions of 10–40 m and ~5 m, respectively. In order to analyse the hydraulic parameters, we generated a digital elevation model (DEM) from two CTX images (D10_031182_1435 and D09_030892_1435) using the method of Kirk et al. (2008). This method uses public-domain Integrated Software for Images and Spectrometers (ISIS) software to pre-process the raw experimental data records (EDRs) before further processing using SocetSet®, a commercially available photogrammetry suite (http://www.socetset.com). During the processing in SocetSet®, we controlled the DTM using MOLA (Mars Orbital Laser Altimeter; Smith et al., 2001) track data, thus allowing us to correlate elevations between topographic datasets of different scales. The output from SocetSet® was an 18 m/ pixel DTM resolving topography of ~50 to 60 m and an orthorectifed CTX image (from D09_030892_1435) at 6 m/pixel. The topographical information for the surrounding area of the outflow channel was derived from the gridded MOLA global DEM with a resolution of 128 pixels/degree (grid cell size ~463 m at equator) (Smith et al., 2001).

Hydraulic modelling was performed on the high resolution stereo-based CTX DTM, using the method described in Kleinhans (2005), in order to calculate the discharge rate of the Kārūn Valles, its volumetric sediment transport rate, and other parameters described in Section 5 aiding to better understand the formative mechanism of the outflow channel. In order to estimate the absolute model age of the fluvial activity, we analysed crater size–frequency distributions (CSFD) on CTX images at a scale of 1:24,000 in ESRI's ArcGIS. Craters were mapped using the CraterTools (Kneissl et al., 2011) extension for the ArcGIS software. The Craterstats 2 software (Michael and Neukum, 2010) was used to model crater-based ages based on the chronology function of Hartmann and Neukum (2001) and the production function of Ivanov (2001). Measured crater populations have been tested for randomness using the method of Michael et al. (2012). The data are plotted as a cumulative presentation of the crater size–frequency distribution. As counting areas, we chose the largest possible zones, however none of the counting areas are large enough to meet the area size of larger than 1000–10,000 km^2 as suggested by Warner et al. (2015). The epoch boundaries are based on Neukum system (Hartmann and Neukum, 2001) as explained in Michael (2013).

3. Regional setting

The fluvial system is located in the mid-latitude highlands of the Terra Cimmeria region between 35° and 37° south. It terminates on the floor of the 200 km diameter Ariadnes Colles basin (Fig. 1). This basin, as well as others in the region, presumably hosted a relative small lake during the Hesperian (Adeli et al., 2015), which was a remnant of the late Noachian-early Hesperian large Eridania paleolake (Irwin et al., 2002). This area shows not only a rich aqueous history, but also Amazonian-aged water/ice-related features (as shown in this study). In fact, ice-related features have been widely reported in the mid-latitude regions of Mars (e.g., Mustard et al., 2001; Kreslavsky and Head, 2002; Head and Marchant, 2003; Hauber et al., 2011; Conway and Balme, 2014). Latitude Dependent Mantle (LDM) is an example of these ice-related landscapes. LDM is a young (formation in the last tens of millions of years; Kostama et al., 2006; Willmes et al., 2012) and ice-rich mantle located at ~30° to 60°latitude in both hemispheres (Mustard et al., 2001). The mobilization of polar ice and its re-deposition due to spin-axis/orbital perturbations has been suggested as LDM formation mechanism at mid-latitudes (e.g., Madeleine et al., 2009). It has been suggested that the post-Noachian valleys in mid-latitudes may be related to the melting of snow and/or ice and subsequent runoff (Fassett and Head, 2007; Howard and Moore, 2011). However, localized events such as melting of ground ice by emplacement of impact ejecta or a transient climate episode (Mangold et al., 2012a) have also been proposed as potential source of water.

In the study area, the Sirenum Fossae graben system extends from east to west over a distance of approximately 2600 km (Wilson and Head, 2002). We can clearly see two main segments of it (Fig. 1a) that are named "northern" and "southern" segments in this study. Kneissl et al. (2015) estimated the main formation time frame for Sirenum Fossae at around $3.44^{+0.1}_{-0.25}$ Ga to $3.46^{+0.046}_{-0.064}$ Ga, and a minimum activity age at 710^{+140}_{-140} Ma. The Sirenum Fossae start in the Tharsis region and terminate at ~200 km to the south of the Ariadnes Colles centre. Its age shows that tectonism in Terra Cimmeria was still active during the middle Amazonian.

4. Geomorphological investigation

We divided the fluvial system under study into three sections, i.e. the upstream, intermediate and downstream sections, based on their different morphological characteristics (Fig. 1a). The upstream section includes the catchment system, crater lakes, alluvial fans, and fan deltas and is composed of two main branches, i.e. an eastern and a western branch. The downstream section includes a valley system that is named Kārūn Valles, which displays a wide alluvial fan, and terminates on the floor of the Ariadnes Colles basin. These two sections are separated by the intermediate section, which is characterized by a flat surface which is cut by the northern segment of the Sirenum Fossae.

4.1. Upstream section

The upstream section of the fluvial system represents the catchment system and hosts two main unnamed channels, which form

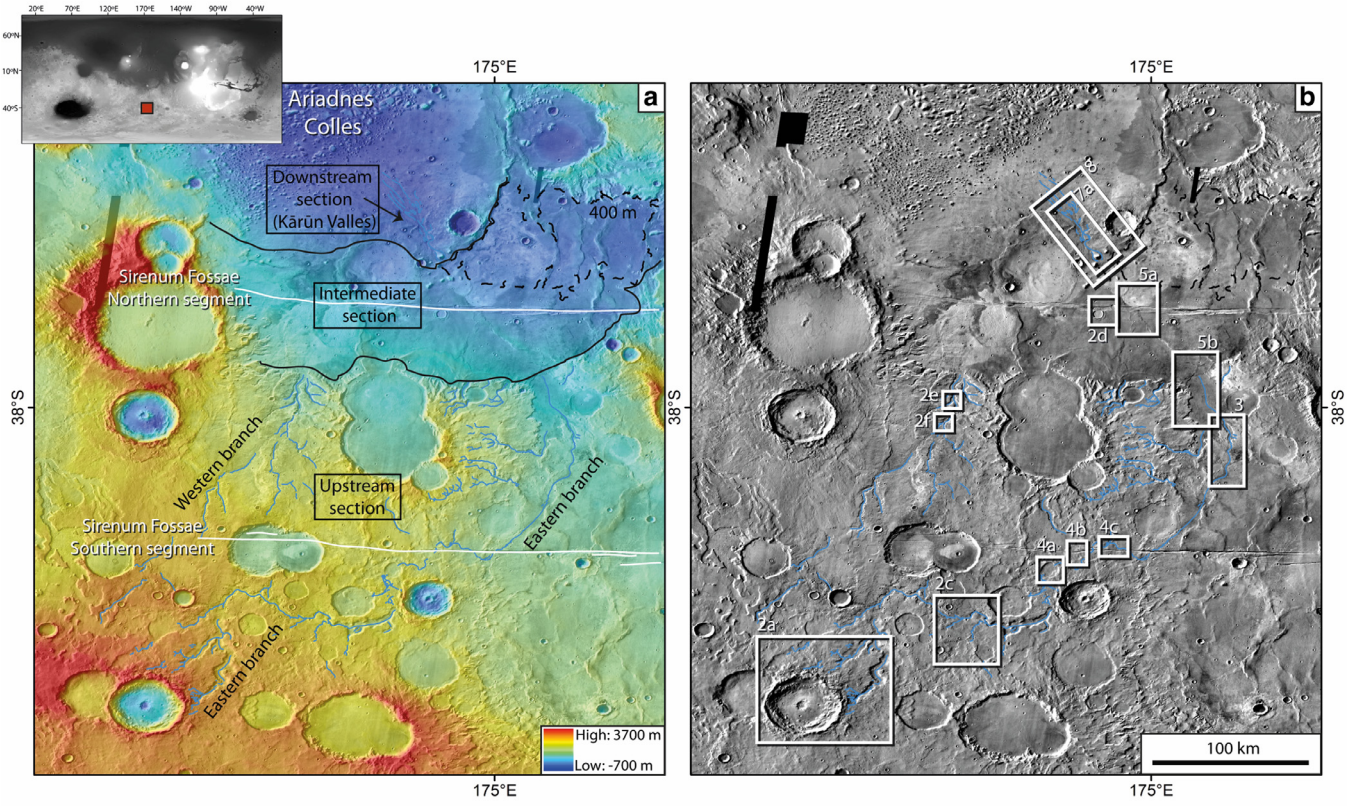

Fig. 1. (a) Study area with main physiographic elements. Colour-coded MOLA digital elevation model at 128 pixels/degree merged with a THEMIS daytime mosaic. The main geomorphologic features are mapped. The fluvial system is represented by solid blue lines, and the eastern and western branches are indicated. Solid black lines show the limit between the intermediate section and the upstream and downstream sections. The Sirenum Fossae are mapped with solid white lines. The location on Mars is shown in the top left inset. (b) THEMIS daytime mosaic with white boxes indicating the locations of most figures in this paper. (For interpretation of the references to colour in this figure, the reader is referred to the web version of this article.)

the eastern and the western branches of the fluvial system. The eastern branch is ~340 km long, has a sinuous plan-view pattern, and is located between impact craters. The western branch is ~220 km in length, appears straight and does not seem to be diverted by pre-existing impact craters. The first observable traces of the fluvial activity appear at an elevation of ~1700 m north and northeast of an impact crater (Fig. 2a). The impact crater has a sharp rim and does not display traces of fluvial activity on its inner rim. The ejecta blanket of this crater is, however, partly eroded. Channels representing the head of the fluvial system appear on the outer wall and ejecta of this crater (Fig. 2a), and therefore they postdate the impact event. A ~5 km-wide deposit is preserved adjacent to a high crater wall (~2000 m height) (Fig. 2b). A narrow channel is most likely originated from this deposit. This channel is linked to the wider channel traceable to the visible heads of the fluvial system. Small channels originating at high elevations join the main eastern and western branches of the fluvial system (Fig. 2c). They have a simple morphology and have no tributaries. They typically start at a local depression and end at the main channel. We have not observed any depositional features such as alluvial fans that are related to these narrow channels. The mentioned depressions are a few kilometres wide (Fig. 2c) and have shallow and irregular shapes, and therefore do not represent old impact craters (Fig. 2c).

On the floor of the western channel, we observe deposits with convex upward surfaces that are partly covered by a smooth mantle that also covers the channel floor area (Fig. 2e). The surface of these deposits is longitudinally fractured (Fig. 2f). These fractures are very common in glacial deposits on Earth, and are called crevasses. They are formed by tensile stresses as response to the ice flow (Benn and Evans, 1998). Next to the northern segment of Sirenum Fossae, two impact craters are filled with smooth-textured materials. The craters rim at the fossae's side is degraded. The filling material is similarly fractured (Fig. 2d). However, these fractures are concentric, running parallel to the crater rim. Additionally, there are longitudinal cracks on the surface of this material, oriented perpendicular to Sirenum Fossae. They may show the creep of this material toward the lower elevation of the fossae.

The floors of the channels in both the western and eastern branches are partly incised by scour marks. Close to the terminus of the eastern branch, where the streamlined islands are well preserved (Fig. 3), we observed a ~2km-wide area with a flat surface that does not display any signs of visible erosion (e.g., fluvial incision). The area is limited downstream by a distinct topographic scarp (Fig. 3). This area may represent a layer of erosion-resistant materials which covers softer materials beneath, a situation which is typical at terrestrial cataracts. Downstream of the scarp we can again follow the channel bed which is characterized by incised erosional features. Another similar feature has also been observed at the north of Sirenum Fossae (Fig. 4a) which is as well distinguished by a flat surface, and a topographic scarp next to which the channel floor is carved by erosion. We infer that these features are paleo-cataracts and represent former waterfalls. At some places we observe eroded banks and erosional islands in the middle of the channel (Fig. 3). About 30 km south of the southern segment of Sirenum Fossae, the channel enters an ancient degraded crater of ~9 km in diameter (Fig. 4b). On the crater floor, there is a fan-shaped deposit with a smooth and flat surface and a distinct frontal scarp, implying a formation as a delta rather than as an alluvial fan, which would be characterized by conical or

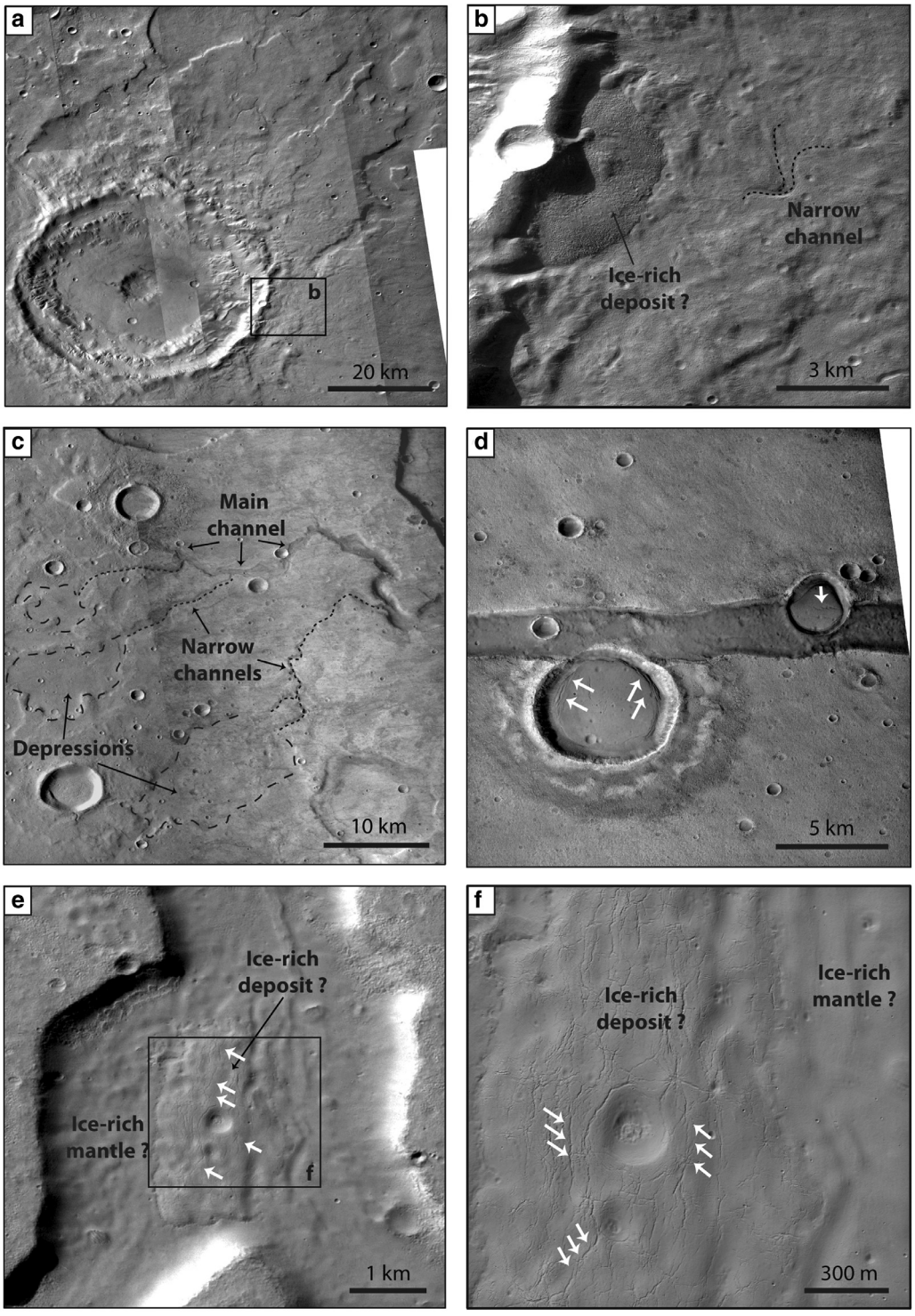

Fig. 2. Morphologic details of the channels in the upstream section. (a) The visible source of the upstream section of the eastern branch. Three channels start at the impact crater and continue toward northeast (detail of CTX P16_007434_1416, G21_026435_1368, P15_006933_1393, D17_033938_1392, and B06_011917_1385). (b) Close-up of the rim of the impact crater seen in (a), showing a well-preserved and possibly ice-rich deposit and a narrow channel, which may be the result of past melt event(s) (detail of CTX P15_006933_1393). (c) Small depressions observed at the head of the narrow channels that fed the main stream (detail of CTX P08_004098_1378 and B06_011851_1397). (d) Two impact craters located next to the northern segment of the Sirenum Fossae. These craters are filled with materials that show characteristics (texture, convex-upward margin, concentric fractures) similar to ice-rich deposits (detail of CTX D10_031182_1435). (e) The floor of the western branch of the upstream section of the fluvial system. An ice-rich deposit is visible on the floor of the channel; it has been partly covered by an ice-rich mantle. The white arrows point to crevasses (detail of CTX B18_016664_1414). (f) Blow up of the surface deposit shown in (e). The limit between the deposit and ice-rich mantle is visible. White arrows point to crevasses (detail of HiRISE ESP_016664_1420). North is up in this and all other figures. See Fig. 1b for locations.

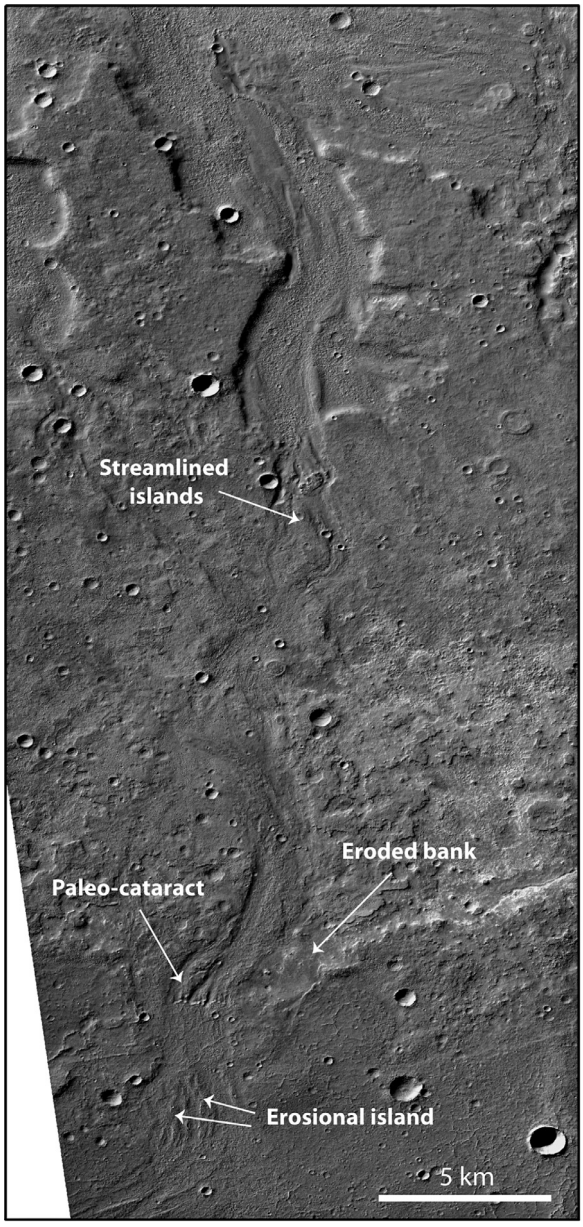

Fig. 3. An area close to the end of the eastern branch of the upstream section. Erosional features are visible on the floor of the fluvial system (detail of CTX G23_027081_1421). Location of this figure is indicated in Fig. 1b.

concave-upward geometry, and a distal margin that grades smoothly into the adjacent plain. An outlet channel leaves the crater on the other side, which is indicative of an open-basin lake (Fassett and Head, 2008). Thus, it suggests the crater hosted a body of water at the time of the fan delta formation.

North and south of Sirenum Fossae, several fan-shaped deposits are observed. Fan-shaped deposit I and II (Fig. 4c) are 1–3 km across, respectively, with gentle and lobate distal margins, which is indicative for an alluvial fan. On top of the fan-shaped I, however, there is a smaller deposit with a steep front and a relatively flat surface (Fig. 4c), which may be a fan delta deposited on top of an alluvial fan. Such a mechanism could occur when an initial alluvial fan is deposited on the floor of a dry basin. When the flow of water continues, consequently a fan delta would form on top. This could not have lasted very long, as otherwise the alluvial fan would be totally covered, which is not the case of the fan-shaped deposit I. The narrow channel terminating at the fan-shaped deposit I (Fig. 4c) incised the Sirenum Fossae's floor, and therefore it formed after the formation of Sirenum Fossae. Here the deposit has been offset vertically rather than laterally, hence the channel dislocated by last activity(s) of the Fossae. The fan-shaped deposit shown in Fig. 4a north of the Sirenum Fossae is more likely to be a fan delta as it appears to have a sharp distal margin. The surface between this fan delta and the adjacent continuation of the fluvial channel is a few kilometres wide. This area may be a small area flooded by water that overflowed east, and formed a flood plain between the upstream fan-shaped deposit and downstream continuation of channelized flow.

4.2. Intermediate section

The intermediate section is about ~85 km long and is located between the eastern branch of the upstream section and Kārūn Valles (downstream section). It does not display any fluvial landforms on is surface and is characterized by two geological units: the bedrock unit south of the northern segment of the Sirenum Fossae, and the mantling unit north of the northern Sirenum Fossae segment which partly overlies the bedrock unit.

4.2.1. Bedrock unit

The bedrock unit appears smooth with bright-tone at CTX resolution (Fig. 5a). It shows several wrinkle ridges that are crosscut by the Sirenum Fossae. The area where the upstream fluvial system terminates is also covered by the bedrock unit, which is clearly incised by the fluvial channel (Fig. 5b). At the terminus of the fluvial system, the bedrock unit reveals low-albedo and light-toned deposits that are polygonally fractured (Fig. 5b). The fractures are a few hundred metres long. The light-toned material within the polygonal fractures reveals also smaller cracks with lengths ranging from 1 to 5 m. The absolute model age of the bedrock unit yields an early Amazonian age of $\sim 1.8^{+0.2}_{-0.2}$ Ga (Fig. 6a) (epoch boundaries are from Michael, 2013).

4.2.2. Mantling unit

The mantling unit has a darker appearance in CTX images as compared to the bedrock unit (Fig. 5a). It is ~5 m thick and covers the area in which the Kārūn Valles are incised. Exposed impact craters range in morphology from nearly pristine (fresh) to degraded; some craters are embayed or partially buried (Fig. 5a). Embayment/burial indicates later resurfacing, which is also notable in our crater size–frequency distribution (CSFD) curve (Fig. 6b) as distinct kink. The base age of $\sim 3.1^{+0.2}_{-0.4}$ Ga refers to the formation age of the pre-existing geological unit whereas the age of $\sim 730^{+40}_{-40}$ Ma represents the formation age of the mantling unit. The material covering the northern segment of the Sirenum Fossae also has very similar appearance as the mantling unit including a low albedo in visible images. This suggests that the mantling unit also covers the ~3 km-wide graben of the northern segment of the Sirenum Fossae (Fig. 5 a).

4.3. Downstream section

4.3.1. Kārūn Valles

The Kārūn Valles (Fig. 7a) extend from southeast to northwest, partly through the ejecta blanket of an impact crater that appears to be relatively fresh (e.g., see crater classification in Mangold et al., 2012b). The Kārūn Valles are the only feature visibly modifying the ejecta blanket, suggesting a recent formation for both; the impact crater and Kārūn Valles. In order to investigate the formative process of the Kārūn Valles, we produced a geomorphological map of these channels and their surrounding area, as shown in Fig. 8.

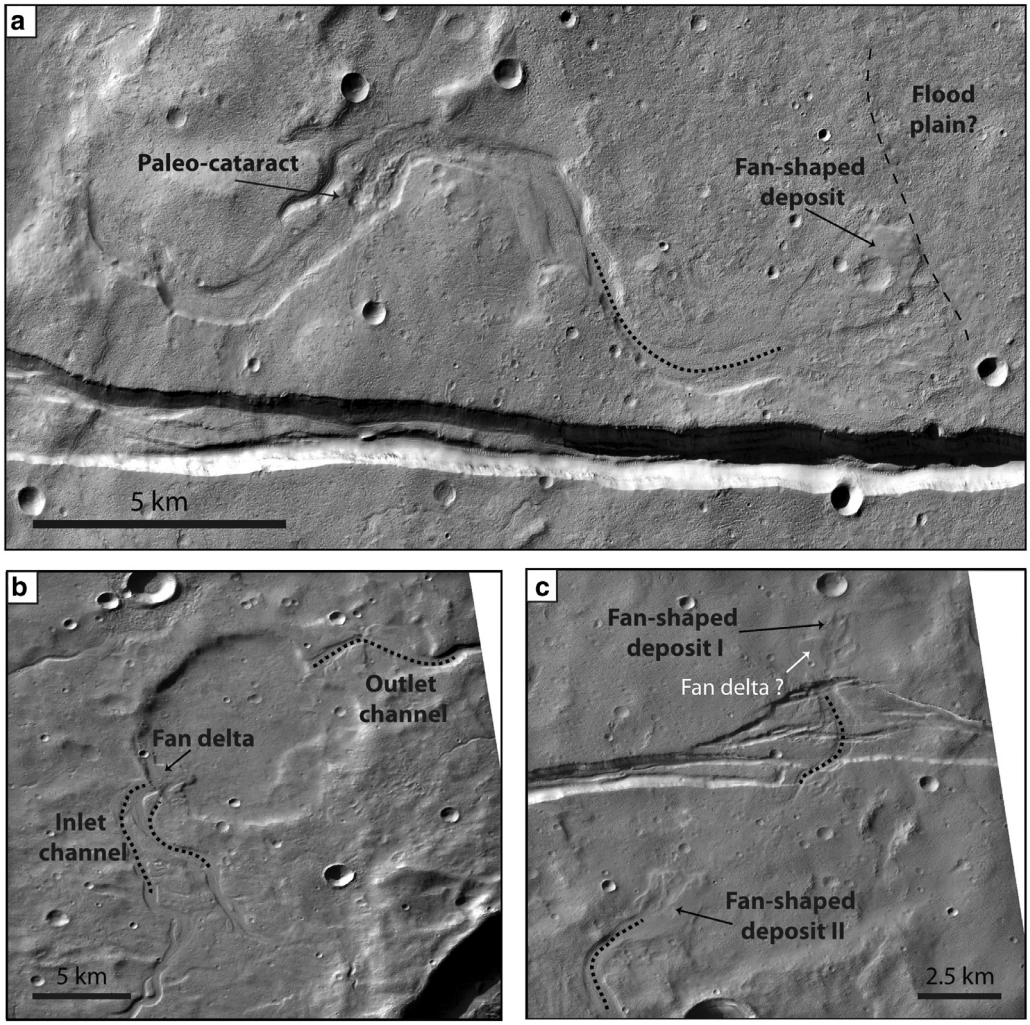

Fig. 4. Fan-shaped deposits in the eastern branch of the upstream section. (a) A part of the eastern fluvial channel that displays a fan-shaped deposit. Note the similarity of the paleo-cataract to the Dry Falls in Channeled Scabland (Washington State, US). A possible flood plain is also shown (detail of CTX F01_036351_1403 and P16_007368_1407). (b) Paleo-crater lake within the eastern branch of the fluvial system, displaying an inlet channel with a fan delta and an outlet channel (detail of CTX P17_007869_1399). (c) Two fan-shaped deposits within the eastern branch (detail of CTX P16_007368_1407). See Fig. 1b for locations.

The Kārūn Valles have a minimum length of ~63 km. Their maximum length is unclear due to the lack of high resolution images. The upstream part of this channel system seems to emanate northeast and southwest of a ~500 m-high hill, located next to the intermediate section. The head of the SW channel cuts the NE channel (Fig. 7a), and therefore the SW channel is younger and was incised more recently than the NE channel. Alternatively, both channel heads may have been active simultaneously but the last or last few outflow events occurred only through the SW channel. The average width of the channel is about 3 km, and its depth ranges between 10 and 30 m. Deep grooves (shown by red lines in Fig. 8) have been observed at the upstream part, as well as along the channel, up to the point where the deposition of the alluvial fan starts. These grooves may indicate scouring of bedrock by high pressure flow in catastrophic floods (Baker et al., 1992).

Along the channel, the ejecta blanket of the crater has been partly removed. Within the channel some remnants are still visible, which resisted the flow and redirected the stream direction (Figs. 7 and 8). The ejecta blanket's remnants are shaped by the erosional processes into streamlined islands, here called erosional remnant islands (EI, Fig. 8). Most EI display an impact crater on one of the sides that may have locally formed obstacles by their rims, increasing the resistance against erosion by the flow. The EI have distinct escarpment that are the result of flow erosion. Between EI 1 and EI 2, and slightly to the north of EI 2 on the eastern wall of the channel, we observe two gaps towards east, debouching into small depressions that may have temporarily hosted standing bodies of water, as indicated with a blue hatched pattern on the map (Fig. 8). Small channels at the head of these gaps show a west-to-east flow direction. These features may indicate bank erosion, which happens when the water level exceeds the channel wall; hence water overflows and erodes the channel wall toward the terrain outside of the channel. Subsequently a small catchment basin may form. On the floor of one of these catchments, a thin layer occurs (Fig. 8) which may have been deposited while the area was filled with water.

The small EI 3 has an elongated shape, oriented in the flow direction with an impact crater at the upstream end. The highly eroded surface and low relief indicate that this EI had been overflowed and that EI 3 has originally been part of EI 4. The morphology of EI 4 indicates it as the rest of the ejecta blanket (see Fig. 8). To the west of EI 4 and 5 there may have been a temporary catchment of water as suggested by the low topography and the deep linear erosional features on the western wall of the channel.

At the head of the Kārūn Valles, on the intermediate section, there is a depression, which fits to the contour line of 400 m

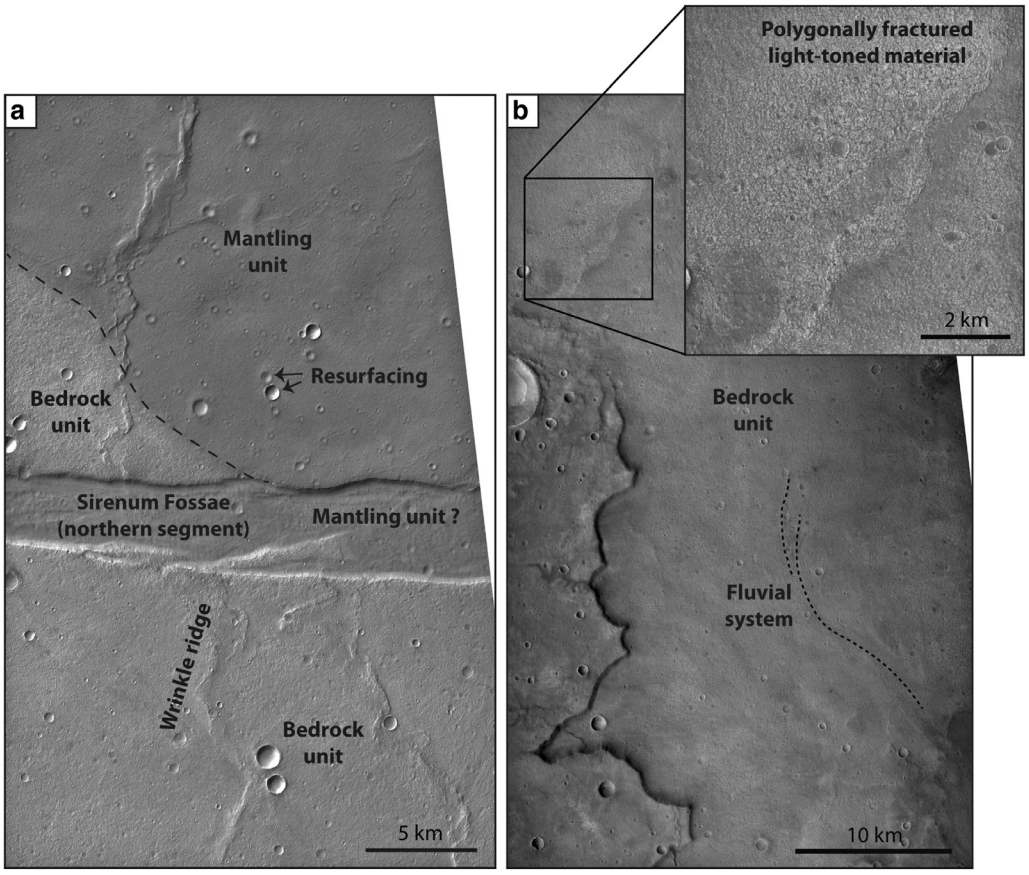

Fig. 5. Morphology of the intermediate section. (a) The two main surface units: bedrock unit and mantling unit. Their contact is indicated by the black dashed line (detail of CTX P17_007658_1420). (b) The eastern branch of the upstream section terminates on the bedrock unit. The blow-up image shows light-toned materials, which are polygonally fractured (detail of CTX D09_030826_1423). See Fig. 1b for location.

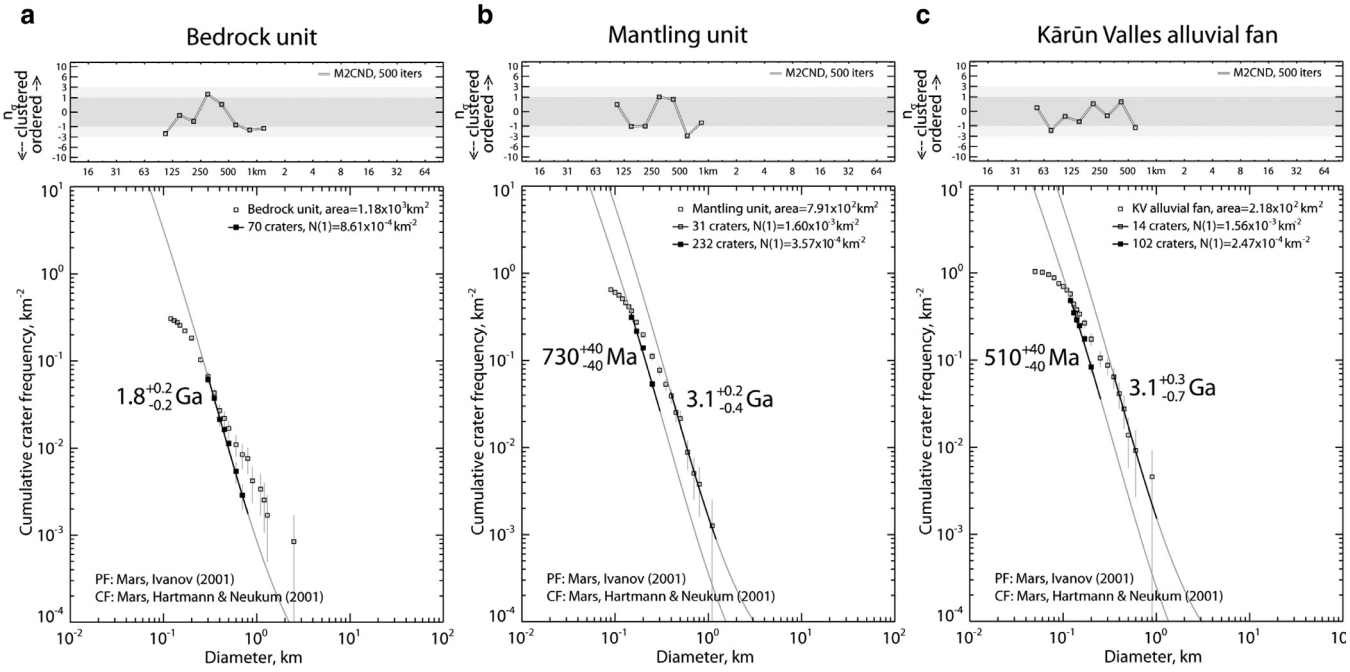

Fig. 6. Absolute model ages corresponding to (a) bedrock unit, (b) mantling unit, and (c) Kārūn Valles alluvial fan. Crater size distributions, randomness analyses, and isochrons are shown.

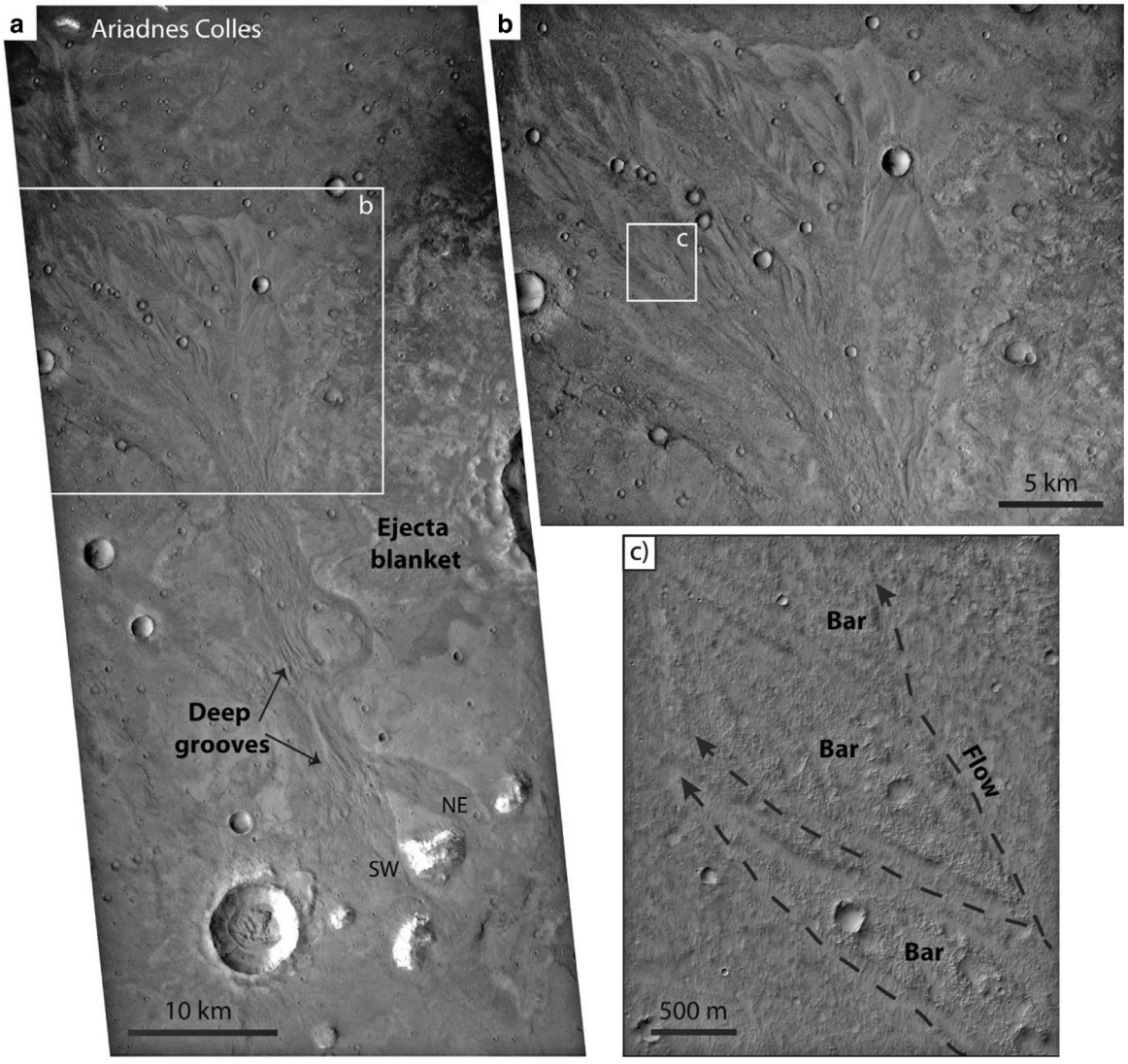

Fig. 7. (a) Morphology of Kārūn Valles located on the rim of the Ariadnes Colles basin. The visible channel head and deep grooves are shown (detail of CTX D10_031182_1435; see Fig. 1b for location). (b) The Kārūn Valles alluvial fan. Note the depositional bars composing the alluvial fan. (c) A zoom on one of the braided bars and the flow direction (detail of HiRISE ESP_043261_1440).

(MOLA DTM) (Fig. 1a). It is located north of the Sirenum Fossae and has a close morphological link with the beginning of the outflow channel. This depression could have hosted a body of water, in liquid or frozen state, the overflow of which could have carved the outflow channel. It should as well be considered that the modern morphology may have been modified by potential Sirenum Fossae activity(s) after the outflow event(s), which could have uplifted or depressed the surface.

4.3.2. Alluvial fan

On the downstream part of the Kārūn Valles there is a wide, low-sloping fan-shaped deposit (Figs. 7 and 8). The deposit contains several bars of various sizes that are all elongated in flow direction. The gentle grade of the bars' distal margins and their concave-upward geometry point toward diverging flow with downstream reducing sediment transport capacity, and depositing a splay-like feature with bars. The bars are found mostly in clusters, around which the main channel has been bifurcated and was divided into numerous narrower channels. The smaller bars of each group are also separated by small channels which reconnect on the downstream side of each bar (Fig. 7c). The complex bars are separated by incisional channels at the larger scale, indicating perhaps a base level drop in the final stages of activity. The bar surfaces show compelling evidence of gradual build-up and migration as multiple scroll bars amalgamated into larger bars. Alternatively, this could also be interpreted as incision by narrow channels. The comparison with data models and experiments (Van De Lageweg et al., 2013; Schuurman and Kleinhans, 2015) shows the former to be more likely. If so, then this, although common in terrestrial rivers, is to our knowledge a unique feature on Mars.

In the main channel, bars are larger but further toward the Ariadnes Colles they become smaller and may have once been part of larger bars and subsequently been divided into smaller ones by erosion. In two locations in the alluvial fan, we observe elongated islands that have sharp scarps and do not exhibit incised channels on their surfaces. A few impact craters are observable on their surfaces (shown by white arrows in Fig. 8). Our observations suggest that these islands formed by erosion rather than deposition and may represent remnants of the ejecta blanket. The crater size–frequency distribution of the entire alluvial fan surface shows a middle Amazonian age of about 510^{+40}_{-40} Ma (Fig. 6c) for the alluvial fan. The model age likely refers to the latest stage of fan formation since previous floods and any pre-existing crater populations would have erased, either by erosion or deposition.

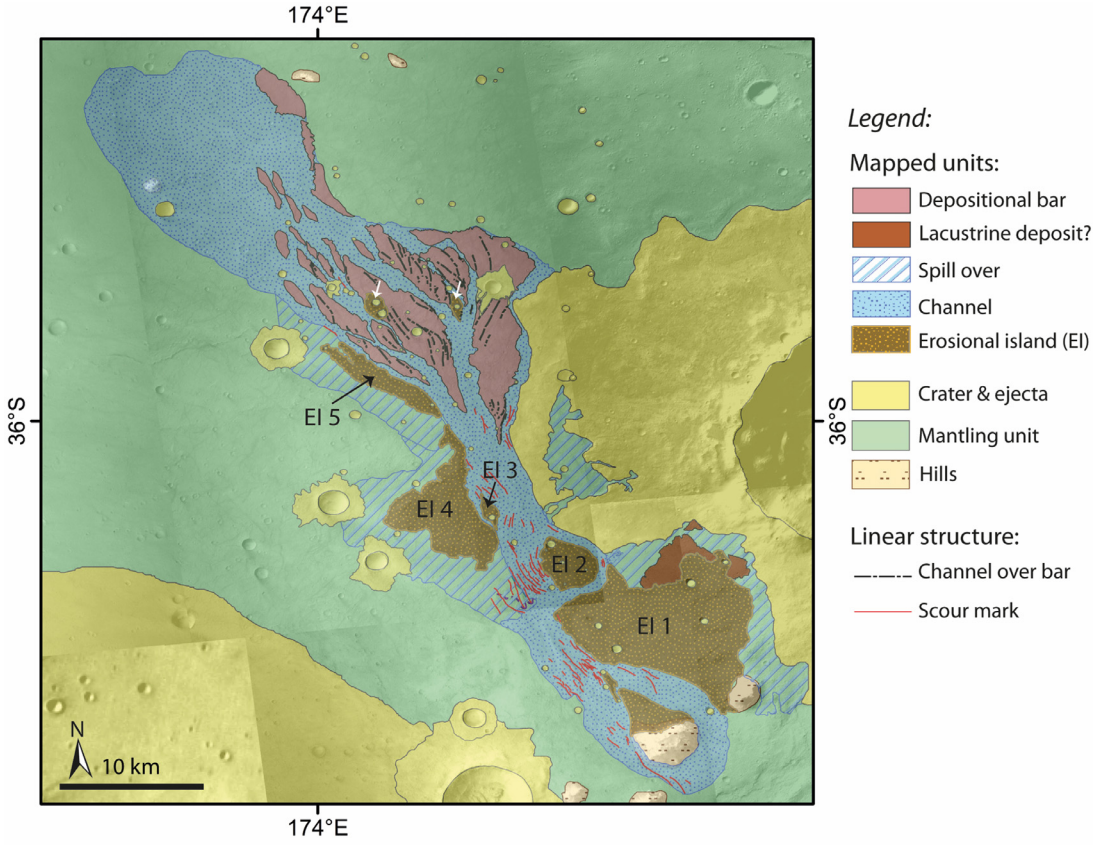

Fig. 8. Geomorphologic map of the Kārūn Valles overlain on CTX and HRSC images. EI stands for erosional remnant island. The white arrows point to the remnants of the ejecta blanket in the alluvial fan. See Fig. 1b for location. (For interpretation of the references to colour in this figure, the reader is referred to the web version of this article.)

5. Hydraulic analysis

5.1. Flow discharge

The hydraulic analysis is essential in order to better understand the channel formation mechanism and potentially the duration and/or periodicity of the flooding, which in turn increases our knowledge about the source of water. On Mars, however, using orbital data for hydraulic modelling is restricted due to the data resolution constraints. In order to calculate the flow discharge rate, we used the method described extensively in Kleinhans (2005) and used in Kleinhans et al. (2010) to calculate the flow discharge and sediment flux under Martian conditions. The flow discharge is given as

$$Q = hWu \tag{1}$$

where h is the depth of the channel, which means the thickness of the water column, W is the channel width, and u is flow velocity averaged over the depth and width of the channel. The channel depth and width can be calculated using the topographic data. The average width of the channel is about 3 km (the width of the channel varies locally from ~1.5 km to ~4.5 km), with minimum and maximum depths of 10 m and 30 m, respectively (based on CTX DTM data, Fig. 9). The flow velocity has to be estimated using a friction law. The most common equations to calculate the flow velocity are the following:

Manning equation:

$$u = \frac{h^{\frac{2}{3}} S^{\frac{1}{2}}}{n} \tag{2}$$

where S is slope of the flow, and n is the Manning roughness coefficient. The Manning equation depends on a dimensional, empirical parameter that includes gravitational acceleration, both of which increase the uncertainty of the results (Kleinhans, 2005; Mangold and Howard, 2013). Therefore, the Darcy–Weisbach equation (Kleinhans, 2005) (Eq. 3) has been used more often in the recent literature. It has also been used in this study:

$$u = \sqrt{\frac{8ghS}{f}} \tag{3}$$

where g is acceleration due to gravity (3.71 m s^{-2} on Mars), and f is a friction factor that depends on channel bed particle size and bed form.

The friction factor can be calculated from a relation that includes the physics-based boundary layer description, and is here calculated for gravel-bed rivers (Wilson et al., 2004) as:

$$f = 8 \Big/ \left(7.515 \left(\frac{h}{D_{50}}\right)^{0.1005} S^{-0.03953} \sigma_g^{-0.1283}\right)^2 \tag{4}$$

where D_{50} is the size at which 50% of clasts are of that size or smaller and σ_g is the geometric standard deviation of the sediment grain size distribution, approximated for logarithmic distributions as:

$$\sigma_g = \frac{1}{2}\left(\frac{D_{84}}{D_{50}} + \frac{D_{50}}{D_{16}}\right) \tag{5}$$

The grain size is an important parameter for the hydraulic analysis, but it cannot be determined based on orbital data. Ground-based rover data acquired on the Martian surface, on the other hand, indicate a variety of grain sizes from gravel (~0.01 m) to sand (~0.002 m) down to clay-sized particles (>60–70-μm resolution limit of MAHLI, the microscopic imager on the Curiosity rover;

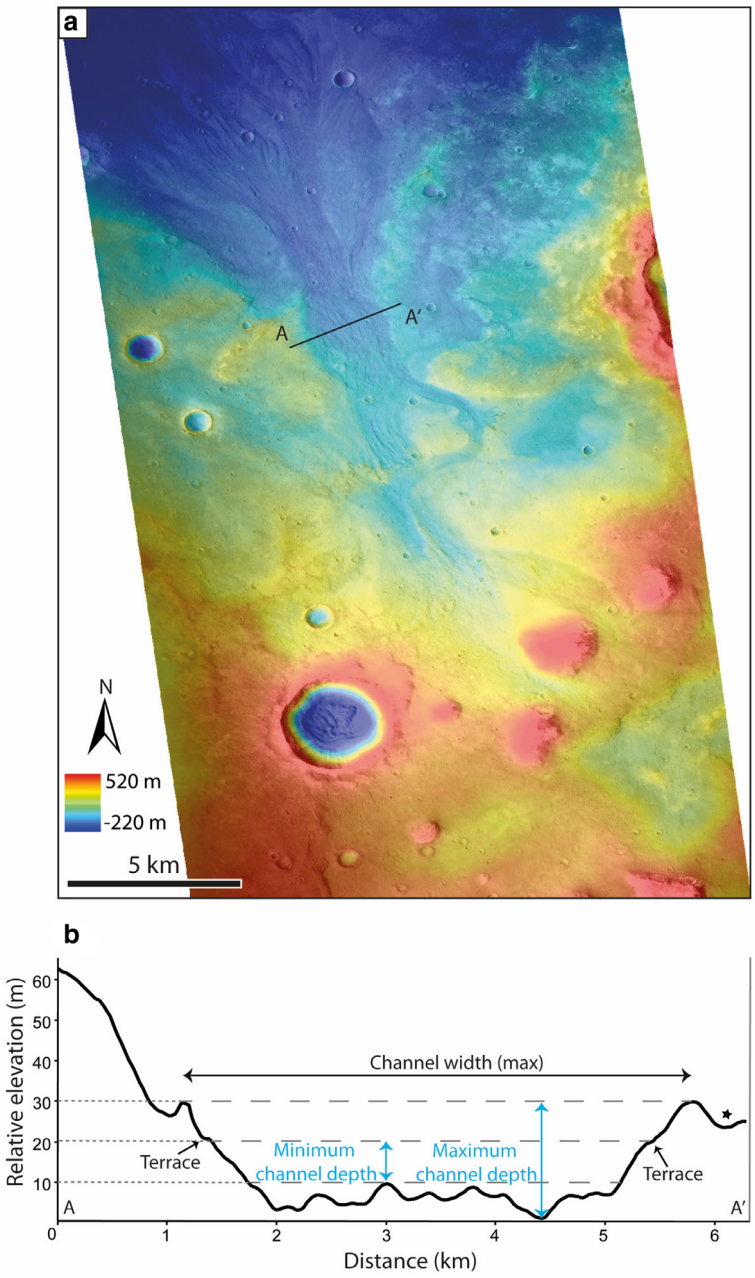

Fig. 9. (a) CTX DEM of Kārūn Valles generated from two CTX images (D10_031182_1435 and D09_030892_1435). The AA' line shows the location of the cross-section presented in (b). (b) Cross-section showing an example of the Kārūn Valles channel depth. Note that the channel width value is the maximum value and not the average value used in our hydraulic modelling. The black star shows the location of a depression which has been mapped as a spill-over region in our map in Fig. 8. (For interpretation of the references to colour in this figure, the reader is referred to the web version of this article.)

Grotzinger et al., 2015). It is, however, difficult to find a comparable geological setting among the sites visited by rovers. The grain size distribution in our study area relates to ejected material, which had been later eroded by fluvial activity and deposited in an alluvial fan. We, therefore, used the average grain size of the fluvial sandstone at the Yellowknife Bay formation as measured by the Curiosity rover (Grotzinger et al., 2015) and assumed a median grain size (D_{50}) of 2 mm. In order to constrain the discharge rate with conservative error margins, we have, in addition, calculated the flow discharge and sediment transport volume for three different average grain sizes which are shown in Table 1. Based on the above channel dimensions, equations, and grain size, we obtained values for the discharge rate of $Q_w = 6.9$ km^3/day for a channel depth of 10 m and $Q_w = 34$ km^3/day for a channel depth of 30 m. It must be noted that these values are order of magnitude estimates given the uncertainty of the friction relation and the chosen particle size. In addition, these values imply bank-full conditions, however, we cannot rule out the possibility of much lower flow depth, at least for a limited time. In order to take this assumption into account, we calculated the discharge rate and other parameters for a case of a 10%-flow-depth, i.e. a flow depth of 1 and 3 m. The results are presented in Table 1b.

5.2. Sediment transport

Estimating the sediment transport rates would give an insight into the channel formation mechanism and event(s) duration. It is essential to compare the removed sediment volume with the

Table 1
Estimation of flow discharge rate, bedload transport, and time-scale needed for Kārūn Valles alluvial fan formation, based on various grain sizes cited in literature (see Section 5). (a) Bank-full condition. (b) 10%-flow-depth condition.

(a) Bank-full condition	Gravel (min)	Gravel (max)	Sand (min)	Sand (max)	Fine grain (min)	Fine grain (max)
Channel depth (m)	10	30	10	30	10	30
Grain size (m)	0.01	0.01	0.002	0.002	0.0005	0.0005
Discharge, Q_w (km^3/day)	7.5	36.8	6.9	34	6.4	31
Total bedload, Q_s (km^3/day)	4.5×10^{-3}	62×10^{-3}	18.9×10^{-3}	261×10^{-3}	64×10^{-3}	897×10^{-3}
Alluvial fan formation time-scale (day)	1100	81	270	19	78	5.6
(b) 10%-flow-depth condition						
Channel depth (m)	1	3	1	3	1	3
Grain size (m)	0.01	0.01	0.002	0.002	0.0005	0.0005
Discharge, Q_w (km^3/day)	0.27	1.3	0.25	1.2	0.23	1.1
Total bedload, Q_s (km^3/day)	0.018×10^{-3}	0.25×10^{-3}	0.07×10^{-3}	1.06×10^{-3}	0.26×10^{-3}	3.65×10^{-3}
Alluvial fan formation time-scale (day)	27×10^4	2×10^4	6.5×10^4	0.47×10^4	1.9×10^4	0.14×10^4

deposited sediment value of the alluvial fan, in order to understand whether any sediment was washed out of the system or was added into the system from the source area, which could consequently increase our understanding about the source of water. We again note that the values are order of magnitude estimates.

Sediment transport can occur as bedload, suspended bedload, and wash load. The suspended load transport regime is most likely dominant in the larger Martian channels whereas the bedload transport becomes more important in smaller channels (Kleinhans et al., 2010). In order to assess the sediment transport, we used the method described in Kleinhans (2005), and calculated the bedload transport, the suspended load transport, and the total load transport. We used the same values as for flow discharge calculation (see Section 5.1.), including channel width, depth, slope, and grain size. The total bedload is calculated using the Engelund and Hansen (EH) predictor, as follows:

$$Q_s = \frac{0.1}{f}\theta^{2.5} \tag{6}$$

where Q_s is nondimentional suspended load transport and f is Darcy–Weisbach coefficient related total roughness. The estimated total bedload for 10 m of channel depth is $Q_s = 18.9 \times 10^{-3}$ km^3/day and for 30 m of channel depth is $Q_s = 261 \times 10^{-3}$ km^3/day. These results are summarized in Table 1a. We have also calculated the sediment transport rate for a 10%-flow-depth condition as shown in Table 1b.

5.3. Time scale

When we have an estimate of the amount of eroded material, deposited material, and the flow discharge rate, we can roughly assess a time window in which the channel had been developed or the alluvial fan had been formed. It can be estimated as (Kleinhans, 2005):

$$T_s = \frac{V_s}{(1-\lambda)Q_s} \tag{7}$$

where V_s is the volume of deposited sediment (in the alluvial fan), λ is the porosity of the sediment that is here assumed to be 0.2. This estimate is based on particle measurements in lander images (see Kleinhans, 2005; Kleinhans et al., 2010 for discussion). This timescale represents the required time to deposit the Kārūn Valles alluvial fan, which has a volume of ~5.04 km^3. Assuming that the fluvial event took place continuously in a given period of time and a bank–full condition, the alluvial fan would need 19–270 days to form, via a channel with 30 m or 10 m of depth, respectively (Table 1a). In case of a 10%-flow-depth condition, the alluvial fan would form in 4700–65,000 days, via flow depth of 3 m or 1 m, respectively (Table 1b). However, we cannot rule out the possibility of several short and repetitive events.

6. Discussion

6.1. The catchment system formation

The fluvial system in Terra Cimmeria is composed of three sections: upstream section forming the catchment system, intermediate section, and downstream section including Kārūn Valles. The fluvial system in Terra Cimmeria reveals a hydraulic mechanism of different erosional and depositional processes. The model absolute age of the bedrock unit in the intermediate section shows an age of $\sim 1.8^{+0.2}_{-0.2}$ Ga, which corresponds to the middle Amazonian, and indicates the maximum age of the fluvial activity. Therefore, the fluvial activity took place at the middle Amazonian or at more recent time. Along the main channel path, we observe narrow valleys, which originate from local depressions (Fig. 2c). The narrow valleys, in our study area, are morphologically very similar (simple morphology, narrow width, few kilometres length, and lack of fan deposits) to Amazonian-aged glaciofluvial valleys described by Fassett et al. (2010), which are interpreted to be related to ice-rich deposits in mid-latitude regions. These valleys are also observed at the eastern channel head, where a ~5 km-wide deposit appears to be linked with a narrow valley to a wider valley (Fig. 2b). The link between deposit, narrow channel, and wider channel may suggest that the deposit is a remnant of a wider ice-rich deposit, which partly melted in the past and incised the narrow valleys, which in turn joined and fed the main fluvial system. This ~5 km-deposit is then remained on a crater rim of ~2000 m of elevation. Alternatively, this deposit's current presence may reveal a potentially long history of re-deposition and disappearance of glacial deposits in the past, in which ice accumulation may have occurred several times at the same location. Nevertheless we suggest that the local depressions, which are located at the head of the narrow channels, have hosted ice or snow deposits, which entirely melted and carved the narrow valleys toward the main water stream.

Next to the northern segment of the Sirenum Fossae, there are two craters, which are filled by smooth and concentric crater fill material. Concentric crater fill material elsewhere on Mars has also been previously interpreted as ice-rich (e.g., Squyres and Carr, 1986; Head et al., 2005; Fassett et al., 2010). This fill material seems to creep toward the topographically lower areas of Sirenum Fossae, similar to the downslope-creeping behaviour of viscous ice-rich deposits in other mid-latitude areas on Mars (e.g., an hourglass-shaped deposit on the eastern Hellas basin rim; Head et al., 2005). Therefore, we infer that the crater filling is remnant of glacial or ice-related material. On the floor of the western fluvial system, there are several deposits with convex-upward cross-sectional profiles that display crevasses on their surfaces (Fig. 2e and f). These deposits are partly covered by a mantle that may be ice-rich and most likely represent the latitude dependent mantle

(LDM, e.g., Mustard et al., 2001; Conway and Balme, 2014). We assume that these deposits are ice-rich, too, due to their prominent morphology, smooth surface and the close link to LDM (Fig. 2e and f). All these well-preserved ice-rich deposits reinforce the possibility of a prolonged glacial history, including the periodic presence and reappearance of surface water, in particular, snow or ice melt, in Terra Cimmeria, during the early to middle Amazonian.

On the intermediate section's surface we have not observed any direct traces of fluvial activities (i.e. channel incision and/or fan-shaped deposits). The morphology of the intermediate section could have been modified by Amazonian tectonic activity related to the Sirenum Fossae. Kneissl et al. (2015) reported that the last tectonic activity of Sirenum Fossae corresponds to $\sim 710^{+140}_{-140}$ Ma, which is almost the age of the mantling unit. Therefore, the intermediate section may have had a different morphology (i.e. surface slope and azimuth) at the time of fluvial activity in Terra Cimmeria, and therefore, it may have been a depression to collect surface runoff. In addition, if the area was glaciated, the Sirenum Fossae-related activity could have been a trigger for collapse and melt of ice, and consequently a catastrophic overflow.

The surface of the bedrock unit is locally polygonally fractured (Fig. 5b). These polygonal fractures, which are found in bright material of the bedrock unit, may indicate a resurfacing mechanism in which liquid water was involved. They are similar to fractures interpreted as desiccation cracks in Mawrth Vallis (e.g., Loizeau et al., 2010), in Terra Sirenum (Adeli et al., 2015), and in former lacustrine settings (e.g., El-Maarry et al., 2013). Therefore, the polygonal cracks in bedrock unit suggest liquid water activity similar to lacustrine environment which may be related to the observed fluvial system or to an earlier water activity in the area. The spatial distribution of the mantling unit is more concentrated in the western and northern part of the intermediate section (Fig. 1b). It is partly covering the bedrock unit at the northern segment of Sirenum Fossae. The Kārūn Valles are incised through the mantling unit and therefore their maximum age is constrained by the age of this unit, which is estimated as $\sim 730^{+40}_{-40}$ Ma, corresponding to the middle Amazonian. The morphological characteristics, distribution, and the Amazonian age suggest that the mantling unit may be a drape of frozen dust. This material has most likely deposited during a middle Amazonian ice age, and reveals one or several recent Amazonian glacial history.

6.2. Kārūn Valles formation

The Kārūn Valles are incised through the ejecta blanket of an impact crater (Fig. 7a). The material removed from the ejecta blanket has been remobilized by the water and was deposited as an alluvial fan. Although the main channel has a straight course (in plan view), there are few islands (EI 1, 2, and 3 in Fig. 8) that redirected the flow. These islands are remnants of the erosion of the adjacent terrace. We do not observe any depositional material around those islands, which implies a high erosion rate in the main channel that did not allow deposition to take place. A high erosion rate is also supported by the deep scour marks on the channel floor (visible in the cross-section of Fig. 9b). This indicates a high sediment transport capacity and sufficient flow strength and sediment load to abrade the bed rock.

Most of alluvial fans on Mars show a lobate shape in plan view (e.g., Moore and Howard, 2005; di Achille et al., 2012). However, on the Kārūn Valles alluvial fan, we observe a bifurcating system rather than a continuously deposited alluvial fan. On Earth, bifurcation occurs in various geological contexts including meandering, anastomosing, and braided rivers, as well as on river deltas with the aforementioned river patterns (Schumm, 1977; Kleinhans et al., 2013). A braided pattern occurs in alleviated conditions when the bars are depositional and shaped inside the river channel by the flow. In such systems, channel migration and instability of channel bifurcations leads to perpetual dynamics with bar growth, bar amalgamation and bar splitting. The Kārūn Valles alluvial fan shows well preserved depositional features, and bars that have been clearly shaped by the flow. The fan is composed of elongated bars and multiple channels that divided and re-joined around the bars. At some places (Fig. 7b and c) bars are connected with each other laterally, suggesting their migration. A few obstacles, most probably remnants of the ejecta blanket, resisted erosion, and sediment was deposited on their lee side. It is clearly observable that the elongation of these obstacles has a different orientation as compared to that of the bars (Fig. 8). The Kārūn Valles alluvial fan is a fan-shaped feature built up from a braided system. Such braiding on Mars has been rarely observed (Matsubara et al., 2015) and points to a unique formation mechanism.

The formation time frame for Kārūn Valles can be constrained by the age of the mantling unit where the Kārūn Valles have been incised into, and the age of the alluvial fan itself. Therefore we infer that the Kārūn Valles formation took place between $\sim 730^{+40}_{-40}$ Ma and 510^{+40}_{-40} Ma, which are the absolute model age estimates of the mantling unit and the alluvial fan, respectively. These ages correspond to the middle Amazonian. The climatic condition (e.g., atmospheric temperature and pressure) during the Amazonian (Madeleine et al., 2009) most probably would not allow liquid water to last or to flow for a long period of time. This fits with our notion that one or several climate changes took place in the recent past and that the appearance of liquid water on the surface may have occurred as a sudden and short event, and water release happened catastrophically.

6.3. Source of water

The erosional features of incised channel floors such as groove marks, cataracts, and streamlined islands; and eroded channel banks in eastern and western branches of the upstream section, as well as in Kārūn Valles, point to highly energetic fluvial activity. The morphology of the depositional features of fan deltas and alluvial fans suggests high energetic and short term events. Similar valleys and landforms of Amazonian age have been reported in other areas in mid-latitudes and been interpreted as being formed by a single and short fluvial episode (Hobley et al., 2014; Salese et al., 2016). The experimental and numerical modelling of de Villiers et al. (2013) demonstrates that deltas with simple morphology and no obvious incisions on their surface form most likely during one short-term aqueous event. Our observations of the small deltas, alluvial fans, and fan-shaped deposits in the upstream section (see Fig. 4) have not shown any incision into their surfaces. The hydraulic modelling of Kārūn Valles also supports a short term event as suggested by our morphological observations and the model of de Villiers et al. (2013). Our calculations point to an event that lasted at least 19–270 days in case of bank-full flow condition in the channel. Although our morphological observations point to energetic flow events which would be more plausible in case of a bank-full or almost bank-full condition, water level variations in the channel are likely, and the flow could have dropped to a fraction of bank-full flow between peaks of high-energy flow events. This would lead to longer flow durations required to carry the sediment, and less dramatic events. In the latter condition the fluvial event could have lasted for tens of thousands of days, e.g., in case of 10% water depth the formative mechanism (in case of a continuous flow) would take only 4700–65,000 days, which is still a geologically short period of time. We do not rule out the possibility of a sequence of multiple episodic short term events. Considering the short duration and catastrophic release of water in combination with our morphological observation of ice-related features, we suggest surface runoff of ice/snow melt as the most likely

water source. Obviously, ice and/or snow accumulation and melting would have happened clearly under different climatic conditions than today. Such climate change(s) may have been triggered by obliquity or orbital variations (Laskar et al., 2004) which mobilized polar ice towards the mid-latitude regions of Mars (Head et al., 2003; Madeleine et al., 2014). An extended ice layer could have covered mid-latitude areas including our study area. This mobilization and re-deposition of ice could have occurred several times and periodically in the past history of Mars (Madeleine et al., 2014).

The depression at the head of Kārūn Valles (see Section 4.3.1. and Fig. 1a) could have hosted an ice-covered lake or a subglacial lake, which collapsed and initiated a catastrophic outflow. Although we have not observed morphological traces of shore line, erosional or depositional features concerning lake or glacial deposit presence, this assumption cannot be ruled out, considering a lake or a glacial deposit, which lasted over a geologically short time. The liquid water collected by the upstream catchment system may have fed the depression at the head of Kārūn Valles, and formed an ice-covered lake under the middle Amazonian atmospheric condition. Alternatively, the depression may have hosted a glacial deposit, which catastrophically collapsed and melted. Catastrophic outburst of large amounts of water in glacier systems has been widely observed on Earth. These are generally referred to by the Icelandic term Jökulhlaups. Jökulhlaups may originate from subglacial sources of water melted by atmospheric processes, geothermal heat or volcanic eruptions (Benn and Evans, 1998; Björnsson, 2009). On Earth, Jökulhlaups generally occur in intervals of weeks to years, and a slightly larger periodicity (e.g., over centuries; Carling et al., 2009) would also be expected under Martian conditions during the Amazonian. An alternative source of water would be rise of ground water. We have not observed any fissure, opening, or collapse zones, but the Sirenum Fossae could have facilitated the process. Groundwater, however, would not explain the distribution of small depressions and ice-rich deposits on various locations and elevations.

7. Conclusions and implications

The morphology of a complex channel system in Terra Cimmeria and the presence of ice-rich deposits on the channel floor strongly suggest that the valleys and channels were incised by liquid water during early to middle Amazonian. The narrow valleys originating at small depressions and remnants of ice-rich material indicate ice/snow melt as water source. The evidence of short term and high energetic event(s), such as deep groove marks, streamlined islands, and morphology of the fan-shaped deposits, enforce the assumption of surface runoff as source of water. Our geologic map and observations of the morphology of the depositional bars in Kārūn Valles alluvial fan show a unique braided depositional pattern typical for terrestrial braided rivers. Our hydraulic and sediment transport modelling is consistent with our morphological observation and suggests that the Kārūn Valles had most likely been carved in one continuous event, which lasted a minimum of few days to few tens of thousands of days, however the possibility of a sequence of several short-term events occurring over a few centuries cannot be ruled out. Kārūn Valles may have been formed by a catastrophic melt of a glacial deposit (i.e., Jökulhlaups) or collapse of an ice-coved lake, which was fed by the upstream catchment and was hosted in the depression that exists at the Kārūn Valles head.

The Amazonian climate is, generally, considered to be globally "cold and dry" (Head et al., 2003) and may have been perturbed by outbursts of water and gas. Observations of significant numbers of Amazonian-aged fluvial channels in the Martian mid-latitudes (e.g., Howard and Moore, 2011; Hobley et al., 2014; Salese et al., 2016) reveal the possibility of the presence of liquid water on the Martian surface during the last 3 Ga. Our observations of glacial-like deposits point to past accumulation(s) of ice/snow on the surface, and the narrow valleys confirms the presence of surface water during early and middle Amazonian. Our study shows a maximum age of $\sim 1.8^{+0.2}_{-0.2}$ Ga, corresponding to the early Amazonian and a minimum age of $\sim 510^{+40}_{-40}$ Ma, corresponding to the middle Amazonian, for the fluvial activity in Terra Cimmeria. Based on our results, we conclude that fluvial activity, perhaps episodic, existed throughout the Amazonian. Liquid water was present in Terra Cimmeria in the Amazonian, and it was abundant enough, although during a short period, to carve over 340 km of fluvial channel, transport sediments and deposit them in alluvial fans and fan deltas. Therefore, the existence of liquid water and fluvial activity on the Martian surface did not completely stop at a specific time, and the transition from a warmer and wetter past climate to today's cold and hyperarid conditions may have been less dramatic than previously thought.

Acknowledgements

This research was supported by the Deutsches Zentrum für Luft- und Raumfahrt (DLR-Berlin). We thank S. Clifford and M.A. de Pablo for their detailed and constructive reviews, which greatly helped to improve the manuscript.

References

Adeli, S., Hauber, E., Le Deit, L., et al., 2015. Geologic evolution of the eastern Eridania basin: Implications for aqueous processes in the southern highlands of Mars. J. Geophys. Res.: Planets 120 (11), 1774–1799. doi:10.1002/2015je004898.
Baker, V.R., Carr, M.H., Gulick, V.C., Williams, C.R., Marley, M.S., 1992. Channels and valley networks. In: Kieffer, H., Kieffer, B., Jakosky, B., Snyder, C., Matthews, M. (Eds.), Mars. Tuscon: University of Arizona Press, pp. 493–522.
Benn, D.I., Evans, D.J.A., 1998. Glaciers and Glaciation. Arnold, London, UK.
Bibring, J.-P., Langevin, Y., Mustard, J.F., et al., 2006. Global mineralogical and aqueous Mars history derived from OMEGA/Mars express data. Science 312, 400–404.
Björnsson, H., 2009. Jökulhlaups in Iceland: Sources, release and drainage. In: Burr, D.M., et al. (Eds.), Megaflooding on Earth and Mars. Cambridge University Press, pp. 50–65.
Carling, P.A., Burr, D.M., Johnsen, T.F., et al., 2009. A review of open-channel megaflood depositional landforms on Earth and Mars. Megaflooding on Earth and Mars. Cambridge University Press.
Carr, M.H., 1995. The martain drainage system and the origin of valley networks and fretted channels. J. Geophys. Res. 100, 7479–7507.
Conway, S.J., Balme, M.R., 2014. Decameter thick remnant glacial ice deposits on Mars. Geophys. Res. Lett. 41 (15), 5402–5409. doi:10.1002/2014gl060314.
Craddock, R.A., Howard, A.D., 2002. The case for rainfall on a warm, wet early Mars. J. Geophys. Res.: Planets 107, 21-1–21-36.
de Villiers, G., Kleinhans, M.G., Postma, G., 2013. Experimental delta formation in crater lakes and implications for interpretation of Martian deltas. J. Geophys. Res.: Planets 118, 651–670.
di Achille, G., Hoke, M.R.T., Rossi, A.P., et al., 2012. Process-response sedimentary modeling of ancient Martian deltas 1: Introduction and case studies. In: Proceedings of Lunar and Planetary Science Conference.
El-Maarry, M.R., Pommerol, A., Thomas, N., 2013. Analysis of polygonal cracking patterns in chloride-bearing terrains on Mars: Indicators of ancient playa settings. J. Geophys. Res.: Planets 118 (11), 2263–2278. doi:10.1002/2013je004463.
Fassett, C.I., Head, J.W., 2007. Valley formation on Martian volcanoes in the Hesperian: Evidence for melting of summit snowpack, caldera lake formation, drainage and erosion on Ceraunius Tholus. Icarus 189, 118–135.
Fassett, C.I., Head, J.W., 2008. Valley network-fed, open-basin lakes on Mars: Distribution and implications for Noachian surface and subsurface hydrology. Icarus 198, 37–56.
Fassett, C.I., Dickson, J.L., Head, J.W., et al., 2010. Supraglacial and proglacial valleys on Amazonian Mars. Icarus 208 (1), 86–100. doi:10.1016/j.icarus.2010.02.021.
Gallagher, C., Balme, M., 2015. Eskers in a complete, wet-based glacial system in the Phlegra Montes region, Mars. Earth Planet. Sci. Lett. 431, 96–109.
Grotzinger, J.P., Gupta, S., Malin, M.C., et al., 2015. Deposition, exhumation, and paleoclimate of an ancient lake deposit, Gale crater, Mars. Science 350 aac7575-1–aac7575-12. doi:10.1126/science.aac7575.
Hartmann, W.K., Neukum, G., 2001. Cratering chronology and the evolution of Mars. Space Sci. Rev. 96, 165–194.
Hauber, E., Reiss, D., Ulrich, M., et al., 2011. Landscape evolution in Martian mid-latitude regions: Insights from analogous periglacial landforms in Svalbard. Geol. Soc. Lond. Spec. Publ. 356, 111–131.

Hauber, E., Platz, T., Reiss, D., et al., 2013. Asynchronous formation of Hesperian and Amazonian-aged deltas on Mars and implications for climate. J. Geophys. Res.: Planets 118, 1529–1544.
Head, J.W., Marchant, D.R., 2003. Cold-based mountain glaciers on Mars: Western Arsia Mons. Geology 31, 641–644.
Head, J.W., Mustard, J.F., Kreslavsky, M.A., et al., 2003. Recent ice ages on Mars. Nature 426, 797–802.
Head, J.W., Neukum, G., Jaumann, R., et al., 2005. Tropical to mid-latitude snow and ice accumulation, flow and glaciation on Mars. Nature 434, 346–351.
Hobley, D.E.J., Howard, A.D., Moore, J.M., 2014. Fresh shallow valleys in the Martian midlatitudes as features formed by meltwater flow beneath ice. J. Geophys. Res.: Planets 119, 128–153.
Howard, A.D., Moore, J.M., 2011. Late Hesperian to early Amazonian midlatitude Martian valleys: Evidence from Newton and Gorgonum basins. J. Geophys. Res.: Planets 116, E05003. doi:10.1029/2010JE003782.
Hynek, B.M., Beach, M., Hoke, M.R.T., 2010. Updated global map of Martian valley networks and implications for climate and hydrologic processes. J. Geophys. Res.: Planets 115, E09008. doi:10.1029/2009JE003548.
Irwin, R.P., Maxwell, T.A., Howard, A.D., et al., 2002. A large Paleolake basin at the head of Ma'adim Vallis, Mars. Science 296, 2209–2212.
Ivanov, B.A., 2001. Mars/Moon cratering rate ratio estimates. Space Sci. Rev. 96, 87–104.
Jaumann, R., Neukum, G., Behnke, T., et al., 2007. The high-resolution stereo camera (HRSC) experiment on Mars Express: Instrument aspects and experiment conduct from interplanetary cruise through the nominal mission. Planet. Space Sci. 55, 928–952. doi:10.1016/j.pss.2006.12.003.
Kirk, R.L., Howington-Kraus, E., Rosiek, M.R., et al., 2008. Ultrahigh resolution topographic mapping of Mars with MRO HiRISE stereo images: Meter-scale slopes of candidate Phoenix landing sites. J. Geophys. Res.: Planets 113, E00A24. doi:10.1029/2007JE003000.
Kleinhans, M.G., 2005. Flow discharge and sediment transport models for estimating a minimum timescale of hydrological activity and channel and delta formation on Mars. J. Geophys. Res.: Planets 110, E12003. doi:10.1029/2005JE002521.
Kleinhans, M.G., van de Kasteele, H.E., Hauber, E., 2010. Palaeoflow reconstruction from fan delta morphology on Mars. Earth Planet. Sci. Lett. 294 (3–4), 378–392. doi:10.1016/j.epsl.2009.11.025.
Kleinhans, M.G., Ferguson, R.I., Lane, S.N., et al., 2013. Splitting rivers at their seams: bifurcations and avulsion. Earth Surf. Process. Landf. 38 (1), 47–61. doi:10.1002/esp.3268.
Kneissl, T., van Gasselt, S., Neukum, G., 2011. Map-projection-independent crater size-frequency determination in GIS environments—New software tool for ArcGIS. Planet. Space Sci. 59, 1243–1254. doi:10.1016/j.pss.2010.03.015.
Kneissl, T., Michael, G.G., Platz, T., et al., 2015. Age determination of linear surface features using the Buffered Crater Counting approach – Case studies of the Sirenum and Fortuna Fossae graben systems on Mars. Icarus 250, 384–394.
Kostama, V.-P., Kreslavsky, M.A., Head, J.W., 2006. Recent high-latitude icy mantle in the northern plains of Mars: Characteristics and ages of emplacement. Geophys. Res. Lett. 33, L11201. doi:10.1029/2006GL025946.
Kreslavsky, M.A., Head, J.W., 2002. Mars: Nature and evolution of young latitude-dependent water-ice-rich mantle. Geophys. Res. Lett. 29, 14-1–14-4. doi:10.1029/2002GL015392.
Laskar, J., Correia, A.C.M., Gastineau, M., et al., 2004. Long term evolution and chaotic diffusion of the insolation quantities of Mars. Icarus 170, 343–364.
Loizeau, D., Mangold, N., Poulet, F., et al., 2010. Stratigraphy in the Mawrth Vallis region through OMEGA, HRSC color imagery and DTM. Icarus 205, 396–418.
Madeleine, J.-B., Forget, F., Head, J.W., et al., 2009. Amazonian northern mid-latitude glaciation on Mars: A proposed climate scenario. Icarus 203, 390–405.
Madeleine, J.-B., Head, J.W., Forget, F., et al., 2014. Recent ice ages on Mars: The role of radiatively active clouds and cloud microphysics. Geophys. Res. Lett. 41, 4873–4879.
Malin, M.C., Edgett, K.S., 2000. Evidence for recent groundwater seepage and surface runoff on Mars. Science 288, 2330–2335.
Malin, M.C., Bell III, J.F., Cantor, B.A., et al., 2007. Context Camera Investigation on board the Mars Reconnaissance Orbiter. J. Geophys. Res. 112 (E5), E05S04. doi:10.1029/2006je002808.
Mangold, N., Carter, J., Poulet, F., et al., 2012a. Late Hesperian aqueous alteration at Majuro crater, Mars. Planet. Space Sci. 72, 18–30.
Mangold, N., Adeli, S., Conway, S., et al., 2012b. A chronology of early Mars climatic evolution from impact crater degradation. J. Geophys. Res.: Planets 117, ED4003. doi:10.1029/2011JE004005.
Mangold, N., Howard, A.D., 2013. Outflow channels with deltaic deposits in Ismenius Lacus, Mars. Icarus 226, 385–401.
Marchant, D.R., Head, J.W., 2007. Antarctic dry valleys: Microclimate zonation, variable geomorphic processes, and implications for assessing climate change on Mars. Icarus 192 (1), 187–222. doi:10.1016/j.icarus.2007.06.018.
Matsubara, Y., Howard, A.D., Burr, D.M., et al., 2015. River meandering on Earth and Mars: A comparative study of Aeolis Dorsa meanders, Mars and possible terrestrial analogs of the Usuktuk River, AK, and the Quinn River, NV. Geomorphology 240, 102–120. doi:10.1016/j.geomorph.2014.08.031.
McEwen, A.S., Ojha, L., Dundas, C.M., et al., 2011. Seasonal flows on warm Martian slopes. Science 333, 740–743. doi:10.1126/science.1204816.
Michael, G.G., Neukum, G., 2010. Planetary surface dating from crater size-frequency distribution measurements: Partial resurfacing events and statistical age uncertainty. Earth Planet. Sci. Lett. 294, 223–229. doi:10.1016/j.epsl.2009.12.041.
Michael, G.G., Platz, T., Kneissl, T., et al., 2012. Planetary surface dating from crater size–frequency distribution measurements: Spatial randomness and clustering. Icarus 218 (1), 169–177. doi:10.1016/j.icarus.2011.11.033.
Michael, G.G., 2013. Planetary surface dating from crater size–frequency distribution measurements: Multiple resurfacing episodes and differential isochron fitting. Icarus 226 (1), 885–890. doi:10.1016/j.icarus.2013.07.004.
Moore, J.M., Howard, A.D., 2005. Large alluvial fans on Mars. J. Geophys. Res.: Planets 110 (E4), E04005. doi:10.1029/2004je002352.
Murchie, S., Arvidson, R., Bedini, P., et al., 2007. Compact Reconnaissance Imaging Spectrometer for Mars (CRISM) on Mars Reconnaissance Orbiter (MRO). J. Geophys. Res. 112 (E5), E05S03. doi:10.1029/2006je002682.
Mustard, J.F., Cooper, C.D., Rifkin, M.K., 2001. Evidence for recent climate change on Mars from the identification of youthful near-surface ground ice. Nature 412, 411–414.
Neukum, G., Jaumann, R., The HRSC Science and Experiment Team, 2004. The high resolution stereo camera of Mars Express. ESA Spec. Publ. 1240, 17–35.
Ojha, L., McEwen, A., Dundas, C., et al., 2014. HiRISE observations of Recurring Slope Lineae (RSL) during southern summer on Mars. Icarus 231, 365–376.
Salese, F., Di Achille, G., Neesemann, A., et al., 2016. Hydrological and sedimentary analyses of well-preserved paleofluvial-paleolacustrine systems at Moa Valles, Mars. J. Geophys. Res.: Planets 121, 194–232.
Schumm, S.A., 1977. The Fluvial System. The Blackburn Press.
Schuurman, F., Kleinhans, M.G., 2015. Bar dynamics and bifurcation evolution in a modelled braided sand-bed river. Earth Surf. Process. Landf. 40 (10), 1318–1333. doi:10.1002/esp.3722.
Smith, D.E., Zuber, M.T., Frey, H.V., et al., 2001. Mars Orbiter Laser Altimeter: Experiment summary after the first year of global mapping of Mars. J. Geophys. Res. 106, 23689–23722.
Squyres, S.W., Carr, M.H., 1986. Geomorphic evidence for the distribution of ground ice on Mars. Science 231, 249–252.
Van De Lageweg, W.I., Van Dijk, W.M., Kleinhans, M.G., 2013. Morphological and stratigraphical signature of floods in a braided gravel-bed river revealed from flume experiments. J. Sediment. Res. 83 (11), 1032–1045. doi:10.2110/jsr.2013.70.
Warner, N.H., Gupta, S., Calef, F., et al., 2015. Minimum effective area for high resolution crater counting of Martian terrains. Icarus 245, 198–240.
Willmes, M., Reiss, D., Hiesinger, H., et al., 2012. Surface age of the ice-dust mantle deposit in Malea Planum, Mars. Planet. Space Sci. 60, 199–206.
Wilson, L., Head, J.W., 2002. Tharsis-radial graben systems as the surface manifestation of plume-related dike intrusion complexes: Models and implications. J. Geophys. Res. 107 (E8), 1-1–1-24. doi:10.1029/2001je001593.
Wilson, L., Ghatan, G.J., Head, J.W., et al., 2004. Mars outflow channels: A reappraisal of the estimation of water flow velocities from water depths, regional slopes, and channel floor properties. J. Geophys. Res.: Planets 109, E09003. doi:10.1029/2004JE002281.
Wordsworth, R.D., Kerber, L., Pierrehumbert, R.T., et al., 2015. Comparison of "warm and wet" and "cold and icy" scenarios for early Mars in a 3-D climate model. J. Geophys. Res.: Planets 120 (6), 1201–1219. doi:10.1002/2015je004787.